

## Time-series analysis of transient chaos

Imre M. Jánosi

*Department of Atomic Physics, Eötvös University, Budapest, Puskin utca 5-7, H-1088, Hungary*

Tamás Tél

*Institute for Theoretical Physics, Eötvös University, Budapest, Puskin utca 5-7, H-1088, Hungary*

(Received 19 August 1993)

A time-series analysis method of transient chaos is worked out which can also be applied to signals of laboratory experiments. The process is based on the construction of a long artificial time series obtained by gluing pieces of many transiently chaotic signals together. This artificial signal represents a long-time motion in the vicinity of the nonattracting chaotic set. Thus all of the well-known numerical methods developed for analyzing permanent chaotic behavior are applicable in a more convenient way than using many short separated time-series pieces. The method is illustrated and its validity is checked by the Hénon map. The nonattracting strange set is reconstructed in the presence of both a periodic and a chaotic attractor, and quantitative characteristics such as dimensions and Lyapunov exponents are determined by means of time-delay embedding methods.

PACS number(s): 05.45.+b, 06.50.Dc

### I. INTRODUCTION: TRANSIENT CHAOS

Signals exhibiting chaotic behavior on finite time scales often occur in nonlinear systems and are called transiently chaotic (for a review see [1]). In such cases one observes a moving around in an apparently chaotic manner and then, rather suddenly, a settling down to an attracting motion which is either periodic or chaotic of another type. If one is studying the asymptotic behavior of such systems only, one loses the interesting, chaotic part contained in the transients.

In systems exhibiting transient chaos there exists in phase space a *nonattracting chaotic set* [1–4], together with an attractor. Trajectories starting from randomly chosen initial points then approach the attractor with probability one. Before reaching it, however, they might come close to the nonattracting set and stay in its vicinity for a shorter or longer time. This results in the appearance of a chaotic motion with a well-defined average lifetime of  $1/\kappa$  where  $\kappa$  is the escape rate, a basic characteristic of the nonattracting chaotic set.

Time-continuous invertible flows underlying physical processes are associated with *invertible* maps which we shall concentrate on in what follows. In such systems the nonattracting set is always a *chaotic saddle*, i.e., an invariant set with stable and unstable manifolds. The saddle and its basin of attraction, i.e., its stable manifold, form a *fractal set of measure zero*. The chaotic saddle itself appears to be the closure of an infinity of periodic orbits [5–7]. It has a fractal structure along *both* its stable and unstable direction in contrast to a chaotic attractor which is always smooth along its unstable direction.

A typical occurrence of transient chaos is in the periodic windows inside the chaotic region. The positivity of the topological entropy then ensures the existence of a nonattracting chaotic set. Such windows occur between

two crisis configurations: a boundary crisis [2] (where a chaotic attractor ceases to exist) and an interior crisis [2] (where a chaotic attractor is suddenly enlarged). The attractor beyond boundary crises is a periodic one, say of period  $m$ , but by increasing a system parameter further it typically undergoes a period doubling bifurcation, and becomes at the accumulation point a chaotic attractor which evolves (via an inverse cascade) into an  $m$ -piece chaotic attractor. Consequently, below and above the accumulation point in the window the nonattracting chaotic set coexists with a periodic and a chaotic attractor, respectively.

Trajectories starting from points of a nonattracting set never leave it and exhibit chaotic motion forever. To hit such a point by a random choice is, however, completely unlikely since the set, together with its basin of attraction, is of zero measure, a fractal. What is observable experimentally is not the chaotic saddle but rather a *small neighborhood* of it and of its stable manifold. Trajectories starting close to the saddle or to its attracting manifold can stay for a long time in a neighborhood of the set and exhibit chaotic properties, but sooner or later they escape. These are the trajectories producing transiently chaotic signals.

The experimental investigation of transient chaos has received, in spite of its relevance, relatively little attention (for a few examples see [8–20]) and, with the exception of a very recent effort [20], has mainly concentrated on determining the averaged chaotic lifetime. In this paper we illustrate that, apart from natural modifications, transient chaos can be analyzed from time series in very much the same manner as permanent chaos. Chaotic saddles underlying transient chaotic dynamics can be reconstructed and their characteristics taken with respect to the natural measure can be determined from time series. To our knowledge, this has not yet been carried

out in any laboratory experiments where the equations of motion of the system are not known.

Suppose we follow one single variable of the system and record the data as a time series. Because of escape from any neighborhood of the strange set, the input of our method has to be an *ensemble* of time series of the pre-selected variable with several initial conditions in some finite domain and with end points on the true attractor. For some purposes, such as, e.g., for reconstructing the chaotic saddle, it is sufficient to have a great number of typically short trajectories with points far away from the attractor. If, however, one is interested in the dimensions and the Lyapunov exponents of the chaotic saddle or in the power spectrum of the transient signal, a single long trajectory might be created via some appropriately chosen gluing procedure. The knowledge of such a long trajectory is also useful because it enables us to take over numerical routines written originally for analyzing permanent chaotic time series.

Our aim is, therefore, to work out the time-series analysis of transient chaos based on the construction of a long artificial signal lying in the vicinity of the chaotic saddle. This signal is in a sense an analogue of the so-called PIM (proper interior maximum) triple trajectory. The PIM triple method introduced by Nusse and Yorke [4] provides in numerical simulations a useful algorithm for generating long trajectories being all the time close to the chaotic saddle. The basic idea is to use a group of initial conditions, follow trajectories for a few steps, and then select two of them which lie closest to and on opposite sides of a branch of the saddle's stable manifold. Between the end points, a set of new initial conditions is taken and the procedure is repeated again and again, leading finally to a long artificial trajectory glued together from short pieces each of which was sufficiently close to the stable manifold. Without knowing the equations of motion, this algorithm is obviously not applicable and cannot be of help for us in the time-series analysis. In a similar spirit, however, we can construct a long artificial signal extracted from an ensemble of transient chaotic time series which will be the central issue of this paper.

Although the method is of general validity, as an illustrative example we use the well-known Hénon map

$$x_{n+1} = 1 - ax_n^2 + by_n, \quad y_{n+1} = x_n, \quad (1)$$

with different parameter sets. This is the most general form of invertible quadratic maps and reflects, thus, faithfully the dynamics associated with systems described by ordinary differential equations.

The paper is organized as follows. In Sec. II we describe the method used for generating a long artificial signal with transient behavior, and the reconstruction of the chaotic saddle is presented. Next, characteristics such as dimensions and the Lyapunov exponent of the nonattracting set are extracted with respect to the natural measure of this strange set. In Sec. IV we discuss interesting fractal properties of the points coming from the gluing procedure. Finally, Sec. V contains a summary and discussion of potential applications.

## II. CONSTRUCTING A LONG ARTIFICIAL SIGNAL

It is worth starting with a brief characterization of transient chaotic signals. The transient part of such time series consists typically of three regions (see Fig. 1): (I) Transient from the initial point to a neighborhood of the nonattracting chaotic set, (II) motion in this neighborhood, and (III) escape to the attractor. For the reconstruction of the nonattracting set, one only needs the points of region II. This part of the signal will be called hereafter the *truncated signal*.

In general, it can be clearly seen by a simple visual observation of the complete signal when the attractor is reached, i.e., where the end point of region III is. Separating regions I and III is less well defined. Region I is associated with the part of the trajectories which approach the chaotic saddle along its stable manifold. The rate of this exponential approach is governed by the first negative Lyapunov exponent  $\lambda_-$  of the saddle. Typically, this number is on the order of unity, therefore in 5–10 steps trajectories come very close to the saddle. Consequently, the length of region I can be chosen between five and ten oscillation periods. Dropping a longer initial part is unnecessary, it leads to information loss without improving the statistics. A strong modification of this rule is needed only if the absolute value of  $\lambda_-$  is very small. Analogously, the length of region III is related to the maximal Lyapunov exponent  $\lambda_{\max}$  of the saddle via the escape along the unstable manifold. Taking the length of region I or region III too short results in the appearance of pieces of the stable or the unstable manifold. This leads to spurious effects and an unfaithful reconstruction of the chaotic saddle. Therefore at any choice of the lengths of regions I and III it is to be checked whether the results depend on these cutoff lengths and one has to use a set for which this is not the case.

One can distinguish three different types of transient chaotic signals, each of which can be split into regions I–III defined above.

(1) Signals settling down on a periodic attractor. It is then rather easy to see when the attractor has been reached, thus defining the end point of region III. As an example, Fig. 1(a) shows a single typical transient chaotic signal of the  $x$  component of the Hénon map at parameters  $a = 1.24$  and  $b = 0.3$ . The attractor is a 6-cycle in this case.

(2) Signals settling down on a multipiece attractor. A complication occurs in such cases since, by working with the selected single variable, the projection of the attractor appears to be a union of intervals which might overlap with the projection of the chaotic saddle. When an element of the time series enters one of these intervals so that it never escapes later any projection interval of the attractor, the trajectory can still be close to the chaotic saddle. By taking the projection, however, some piece of information is lost, and we cannot do better than considering this element to be the end point of region III in such cases. In Fig. 1(b) a transient signal of the Hénon map is plotted at parameter values  $a = 1.2715$  and  $b = 0.3$ . In this case, the chaotic attractor consists of seven pieces,

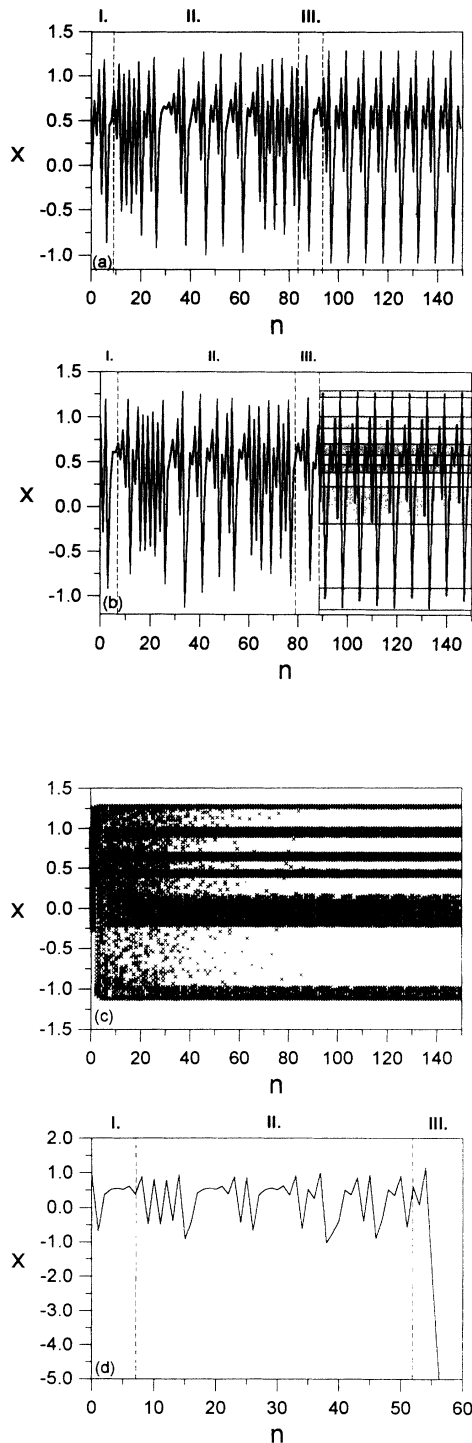


FIG. 1. Typical transient signals generated by variable  $x$  of the Hénon map. (a) Signal settling down on a period-6 attractor,  $a = 1.240$ ,  $b = 0.3$ . The initial point is  $x_0 = 0.92$ ,  $y_0 = 0$ . (b) Signal settling down on a multipiece chaotic attractor,  $a = 1.2715$ ,  $b = 0.3$ . The initial point is  $x_0 = 0.06$ ,  $y_0 = 0$ . The shaded stripes represent the projection of the seven-piece chaotic attractor to the  $x$  axis. (c) An ensemble of 200 transient chaotic trajectories belonging to uniformly distributed initial points in the interval  $|x| < 0.5$ ,  $y = 0$  at the same parameters as in (b). (d) Signal going to infinity at parameters  $a = 2.0$  and  $b = 0.3$ . The starting point is  $x_0 = 0.930\ 092$ ,  $y_0 = 0$ .

which fall in this projection on six separated intervals. By following an ensemble of trajectories in the same plot [see Fig. 1(c)], these intervals are filled up with points of the asymptotic motion. One clearly sees also how the gaps in between become with increasing time less and less populated by the transients. The length of the densely populated region in the gaps gives a fairly good estimate to the averaged transient chaotic lifetime.

(3) Signals settling down on an attractor lying far away from the chaotic saddle so that it can be considered to be at infinity. The end point of region III is then defined by an  $x$  coordinate which first falls out of a preselected interval covering the projection of the chaotic saddle. A typical transient signal is shown in Fig. 1(d) generated by the Hénon map at the parameters  $a = 2.0$  and  $b = 0.3$ . The escape from the strange set is obvious by observing the very fast divergence to minus infinity where the attractor is situated.

In order to concentrate on the dynamics associated with the chaotic saddle, we have to delete those typically long parts of the signals which lie close to the attractor, as well as regions I and III. Thus an ensemble of truncated signals arises. The average length of these truncated signals is on the order of the average transient lifetime  $1/\kappa$ .

Our aim is to construct from these pieces an *artificial time series* representing the long-time motion in a close vicinity of the chaotic saddle. The advantage of having it will be that this time series can then be analyzed by standard embedding techniques [22]. As has been pointed out by Kantz and Grassberger [3], the use of an ensemble enables us to generate a measure which can be considered to be the *natural measure* on the chaotic saddle. Thus we expect that the artificial time series constructed from the ensemble of short signals will also define the natural measure, and statistical characteristics of the chaotic saddle computed from it will be taken with respect to this measure.

The most naive approach is to simply glue together all the truncated signals without taking care of adjusting the ending and starting points. The effectiveness of this can be checked by constructing the invariant set on a Poincaré plane of a low-dimensional case and comparing it with known results. In Fig. 2 we have plotted the first return map of a long artificial time series produced by gluing together 4000 truncated signals of the Hénon map at the parameter values of Fig. 1(c). A low-dimensional object, the chaotic saddle is clearly observable together with some scattered points. These points (the cloud) are the consequence of the gluing procedure applied to produce the long-time series. In order to understand the origin of the cloud we argue as follows. Take two truncated time series of the long signal [see Fig. 3(a)]. It is obvious that the jump between the end point of the first segment and the first point of the second segment generates a cloud point which does not belong to a close neighborhood of the saddle. Comparing the saddle of Fig. 2 with a saddle obtained by direct numerical iteration, the only difference is that gaps of small size along the unstable direction are filled up, which is a consequence of the gluing procedure again.

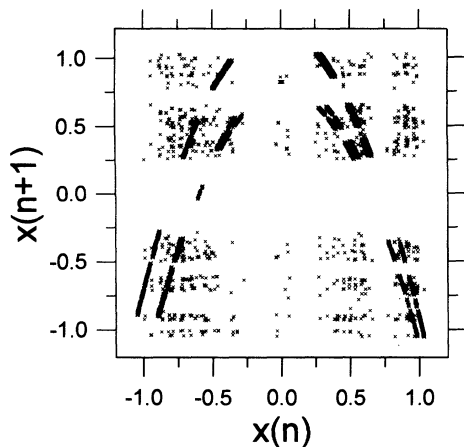


FIG. 2. First return map of a long artificial time series generated by 4000 truncated signals of the Hénon map at parameter values  $a = 2.0$ ,  $b = 0.3$  with uniformly distributed initial points in the square  $|x|, |y| < 0.5$ . The number of points discarded at the beginning (region I) and before reaching the attractor (region III) was chosen to be 5 and 6, respectively. The high density regions are parts of the chaotic saddle.

The next step is to avoid the appearance of these artificial cloud points so that we end up with one long signal of the transient dynamics. A possible method is based on a *matching* of the truncated signals. An effective matching condition is the following: Choose a point in the truncated time series which has a value close enough to the end point of the previous segment, discard the intermediate points, and glue the remaining part to the end point of the preceding segment so that

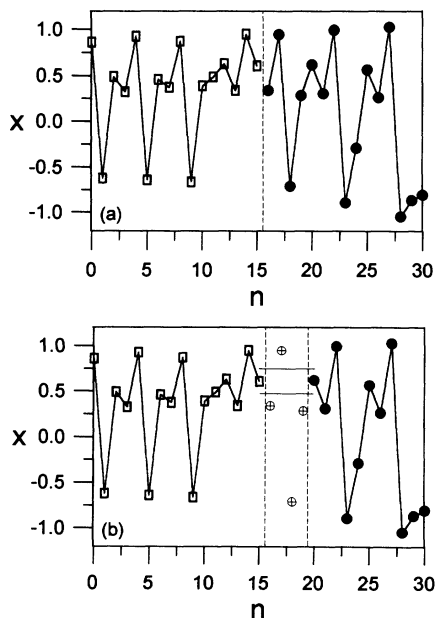


FIG. 3. (a) Two short truncated time series of the time series used in constructing Fig. 2. The gluing procedure is represented by a vertical line. (b) Illustration of the matching procedure. The points represented by open circles are discarded (see text).

$$x_g^{(n)} = x_e^{(n-1)}(1 \pm c) \quad (2)$$

Here  $x_g^{(n)}$  is the gluing point of the  $n$ th truncated time series,  $x_e^{(n-1)}$  denotes the end point of the preceding segment, and  $c$  is the allowed error range. What one obtains in this way can be considered as the desired long artificial time series with transient chaotic properties. The matching procedure is demonstrated in Fig. 3(b), and the result obtained for the chaotic saddle is shown in Fig. 4. Here the first return map of the time series of Fig. 2 is plotted after applying the matching rule (2) with  $c = 0.1$ . Almost all of the false cloud points disappeared. It is worth noting that the matching procedure removes the cloud points on the relative scale of the matching error only. Using a nonzero value of  $c$ , it is never possible to reconstruct the chaotic saddle with the same accuracy as with a direct numerical calculation.

Naturally, the matching process results in decreasing the number of data. A possible quantitative measure of this is the data reduction factor  $g$  which is the portion of data points that survived the matching procedure. Figure 5 shows the dependence of the data reduction factor ( $g$ ) on the matching error ( $c$ ).

Some more advanced matching procedures could also be used, such as, for example, pattern matching. In this case not a single value of a truncated time series is to be matched to a single end point of the preceding segment, rather a pattern formed by two or three succeeding points is to be compared with the end pattern of the former segment. It is interesting to note that in our case neither the two-point nor the three-point matching procedure improves significantly the results compared with the single-point matching. This is so because trajectories starting from close initial points remain quite close to each other for a few time steps. Applying longer-pattern matching is meaningless because it may cause a drastic dropping of the number of data without improving the resolution of the reconstruction.

The algorithm can, of course, also be applied to cases where the attractor is close to the chaotic saddle. Fig-

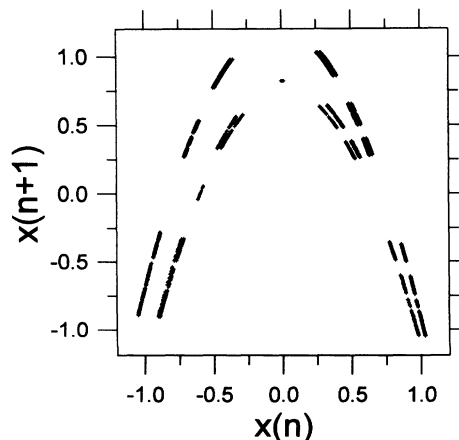


FIG. 4. First return map of the time series of Fig. 2 after applying the matching condition Eq. (2) with the value  $c = 0.1$ .

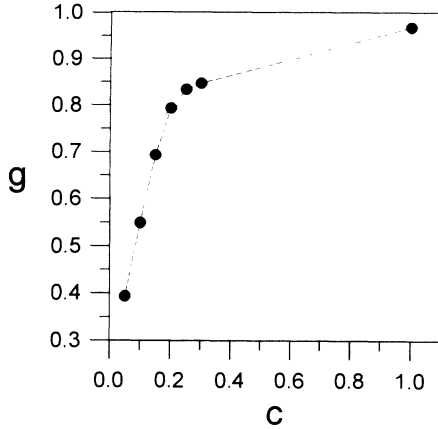


FIG. 5. Data reduction factor ( $g$ ) vs different matching error values ( $c$ ) [see Eq. (2)] applied to the ensemble of truncated time series used in Figs. 2 and 4.

Figure 6 illustrates the result obtained at the parameters of Fig. 2(b). The applied matching error in Eq. (2) was  $c = 0.15$ . The thick and thin parts of the object represent the chaotic attractor and the chaotic saddle, respectively.

### III. EXTRACTING CHARACTERISTICS OF THE SADDLE

As a next step of the time-series analysis, one can determine, for example, the dimension of the chaotic saddle. There are several well-known methods for measuring the dimension of a fractal object, such as the simple box-counting method [21] or the correlation dimension calculation [22,24,25]. In order to compare the two methods we carried out several calculations. An example is shown in Fig. 7 for the case when the attractor is a 6-cycle. The

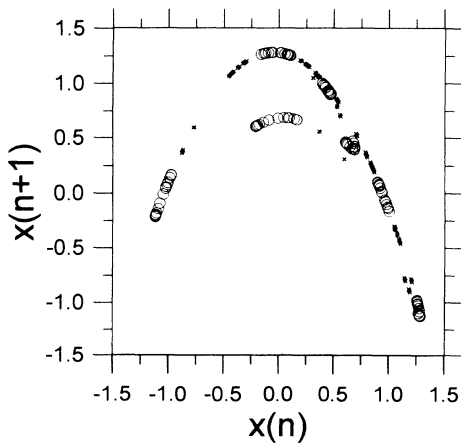


FIG. 6. Reconstruction of the chaotic saddle (crosses) of the Hénon map in the presence of a chaotic attractor (circles). The parameters are  $a = 1.2715$  and  $b = 0.3$ . Four thousand truncated signals were used and the length of regions I and III was chosen to be 4 and 5, respectively. Cloud points have been filtered out by using the matching procedure [Eq. (2)] with  $c = 0.15$ .

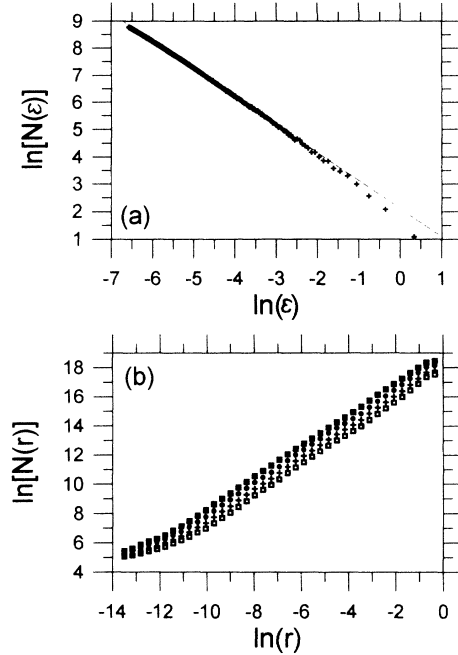


FIG. 7. (a) Result of the box-counting calculation of the chaotic saddle at parameters  $a = 1.240$  and  $b = 0.3$  [the case of Fig. 2(a)]. The slope of the dashed line is  $-1.05$ . (b) Correlation sums for the same strange set. Curves denoted by different symbols correspond, from top to bottom, to embeddings in dimensions from two to five. The slope of the parallel straight line segments is  $1.07$ .

number of two-dimensional boxes  $N(\epsilon)$  of linear size  $\epsilon$  needed to cover the chaotic saddle is plotted in Fig. 7(a). The best power fit yields the dimension

$$D_{\text{box}} = 1.05 \pm 0.1 \quad .$$

The relatively large error comes on one hand from the gluing procedure, on the other hand from the unavoidable effect that the time series tests a neighborhood of the nonattracting chaotic set only. Figure 7(b) shows the result obtained via the embedding technique. A phase point  $\mathbf{p}_i$  is defined by the  $m$ -dimensional time-delay vector

$$\mathbf{p}_i = (x_{i-m+1}, \dots, x_{i-1}, x_i) \quad , \quad (3)$$

as usual [22]. The correlation sum  $N(r)$  is obtained by counting the number of neighboring phase points which are closer to each other than a distance  $r$ :

$$N(r) = \{\text{number of pairs: } |\mathbf{p}_i - \mathbf{p}_j| < r\} \quad .$$

In the scaling region  $r \ll 1$ , the correlation dimension  $D_{\text{cor}}$  is given by the exponent of the best power fit to the correlation sum  $N(r)$  vs  $r$ . As is clearly seen in Fig. 7(b), the embedding process is characterized by correlation sums, the graphs of which run parallel to each other on a log-log plot for  $2 \leq d \leq 5$ . The correlation dimension extracted from these is  $D_{\text{cor}} = 1.07 \pm 0.05$ .

In order to check the reliability of these methods we compared the results of the time-series analysis to a di-

rect dimensional calculation of the Hénon saddle at the parameters  $a = 2.0$  and  $b = 0.3$ . The algorithm is based on the investigation of the fractal structure of the stable manifold. Observing the way the bundles of the manifold split into narrower and narrower bundles by increasing the resolution, one can derive quantitative characteristics of the chaotic saddle [23]. For the generalized dimensions  $D_q$  with  $q = 0, 1, 2$  taken with respect to the natural measure of the nonattracting set this direct method yields  $D_0 = 0.898 \pm 0.003$ ,  $D_1 = 0.895 \pm 0.003$ , and  $D_2 = 0.891 \pm 0.003$  [23]. By reconstructing the strange set at the same parameters with the embedding method, determining its box-counting dimension on the Poincaré plane, and its correlation dimension from the correlation integral, we obtain  $D_{\text{box}} = 0.85 \pm 0.1$ ,  $D_{\text{cor}} = 0.90 \pm 0.02$ . The agreement with the results of the direct method is satisfactory, the quantities  $D_0$  and  $D_{\text{box}}$  as well as  $D_2$  and  $D_{\text{cor}}$  coincide within the error bars.

Next, we turn to the determination of Lyapunov exponents [26–28]. To extract the maximal Lyapunov exponent from our “experimental” time series we have applied the very simple algorithm of Kantz [29] which makes use of the statistical properties of the local divergence rates of nearby trajectories. Without the details, the outline of the method is the following.

Take an arbitrary point of the time series in  $m$ -dimensional delay coordinates  $\mathbf{p}_i$  [see Eq. (3)]. All delay vectors of the series falling into a  $\delta$  neighborhood of  $\mathbf{p}_i$  will be considered as the beginning of neighboring trajectories, which are simply given by the consecutive points of the time series. Let us consider a reference trajectory  $\mathbf{p}_i(\tau)$  starting with  $\mathbf{p}_i$ . A distance  $\mathcal{D}$  between this reference trajectory and a neighboring one  $\mathbf{p}_j(\tau)$  with an initial point  $\mathbf{p}_j$  in a  $\delta$  neighborhood of  $\mathbf{p}_i$  can be defined at time  $\tau$  by

$$\mathcal{D}(\mathbf{p}_i, \mathbf{p}_j, \tau) = |x_{i+\tau} - x_{j+\tau}| ,$$

i.e., by taking the difference of the  $\tau$ th *scalar* component of the two trajectories. In order to measure the maximal Lyapunov exponent one should fix  $i$ , search for all  $\delta$  neighbors of  $\mathbf{p}_i$ , and compute the average of the distances between all neighboring trajectories and the reference trajectory as a function of  $\tau$ . To get rid of the fluctuations due to the projections of the difference vectors in true phase space onto a one-dimensional subspace and to the local effective exponents, one should average the logarithm of the distances defined above over the full length  $N$  of the time series:

$$S(\tau) = \frac{1}{N} \sum_{i=1}^N \ln \left( \frac{1}{n} \sum_{j \in \delta} \mathcal{D}(\mathbf{p}_i, \mathbf{p}_j, \tau) \right) , \quad (4)$$

where  $n$  denotes the number of neighbors in the  $\delta$  neighborhood of the reference vector  $\mathbf{p}_i$ . For a range of  $\tau$ ,  $S(\tau)$  increases linearly with a slope  $\lambda_{\text{max}}$  which is the estimate to the maximal Lyapunov exponent (for details see [29]).

The validity of this method has been checked by computing the maximal exponents of several well-known attractors — such as the logistic map, the Hénon map, and the Lorenz attractor with different parameters —

and the results were convincing [29]. We concentrate here on the characteristics of chaotic saddles. Plotted in Fig. 8 is the quantity  $S(\tau)$  vs  $\tau$  for the artificial time series given by the Hénon map at two parameter ranges. At parameters  $a = 1.2715$  and  $b = 1.3$  (seven-piece attractor range) the estimation gives  $\lambda_{\text{max}} = 0.585 \pm 0.010$ . Note that this value is much larger than the maximal Lyapunov exponent of the seven-piece chaotic attractor  $\lambda_{\text{max}}^{(a)} = 0.057$ . This shows that the chaotic saddles in periodic windows are more unstable, i.e., “more chaotic” objects than the chaotic attractors. For the parameters  $a = 2.0$  and  $b = 0.3$  (attractor at minus infinity) the result is  $\lambda_{\text{max}} = 0.83 \pm 0.03$  (Fig. 8). There exists a famous formula [3] expressing the information dimension  $D_1^{(u)}$  along the unstable manifold in terms of the escape rate  $\kappa$  and the maximal Lyapunov exponent  $\lambda_{\text{max}}$  of the saddle in three-dimensional flows or two-dimensional maps as

$$D_1^{(u)} = 1 - \frac{\kappa}{\lambda_{\text{max}}} .$$

At the parameter setting  $a = 2.0$  and  $b = 0.3$  we find, by observing the exponential distribution of the lengths of truncated signals, that  $\kappa = 0.305 \pm 0.002$ . Thus we obtain the approximate value  $D_1^{(u)} \simeq 0.63$  which is expected to be close to the fractal dimension  $D_0^{(u)}$ . In view of the fact that the total dimension is the sum of the partial ones, the fractal dimension along the stable direction can be estimated as  $D_0^{(s)} \simeq 0.27$ .

The detailed investigation of the divergence properties of trajectories near a chaotic saddle is not presented here, rather we intended strictly to demonstrate the advantage of using a long-time series in computations like this.

#### IV. THE CLOUD POINTS

It is interesting to investigate the structure of the cloud emerging from nonmatched gluing points (see Fig. 2).

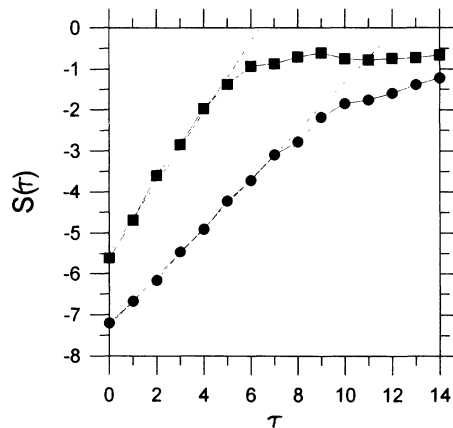


FIG. 8.  $S(\tau)$  vs  $\tau$  for the artificial long-time series of the chaotic saddles [see Eq. (4)]. Upper curve:  $a = 2.0$ ,  $b = 0.3$ ,  $\delta = 0.002$ ,  $N = 4000$ , the slope of the fit is 0.83; lower curve:  $a = 1.2715$ ,  $b = 0.3$ ,  $\delta = 0.001$ ,  $N = 4000$ , the slope of the fitted line is 0.585. Two-dimensional time-delay embedding was used for the search of neighboring trajectories in both cases.

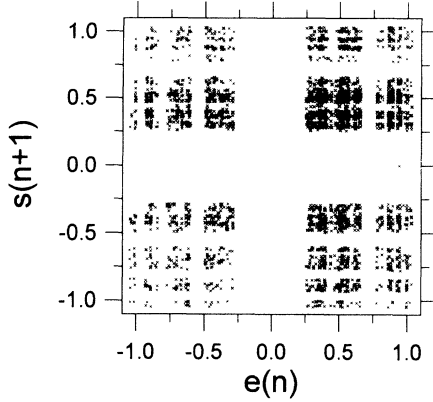


FIG. 9. The cloud of the nonmatching gluing procedure separated from the chaotic saddle at parameters  $a = 2.0$  and  $b = 0.3$  (see text). An ensemble of 10 000 truncated signals was taken.

Figure 9 shows the cloud separately which was obtained by plotting just the end points of the truncated time series versus the starting point of the next truncated time series. The obvious fractal structure can be understood by observing that both the end points and the starting points can take on any values on the projection of the chaotic saddle on the  $x$  axis. Consequently, the cloud is the *direct product* of the projection of the chaotic saddle on the  $x$  axis with itself. The fractal dimension of a projection coincides with the fractal dimension of the entire set for sufficiently rarified fractals [21]. Otherwise, the dimension of the projection is the same as the dimension of the projection space (1 in our case). Since the dimension of a direct product is the sum of partial dimensions, the fractal dimension of the cloud on a Poincaré plane is  $\min(2D_0, 2)$  where  $D_0$  is the fractal dimension of the chaotic saddle. Figure 10 shows the results obtained for the box-counting dimension of the cloud of Fig. 9. The

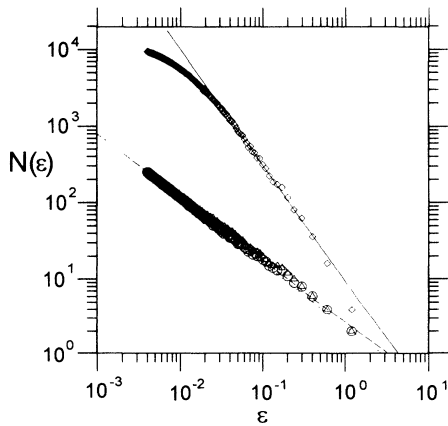


FIG. 10. Box-counting results for the cloud of Fig. 9. The upper curve corresponds to a covering of the set by two-dimensional squares of linear size  $\epsilon$ , while the lower curves correspond to the covering of the one-dimensional projections by intervals of the same size. The slope of the full line (upper curve) is  $-1.5$ . That of the dashed line ( $x$  projection) and the dotted line ( $y$  projection) is  $-0.78$  and  $-0.84$ , respectively.

upper curve corresponds to the two-dimensional covering of the entire cloud, and yields  $D_{\text{box}}^{(\text{cloud})} = 1.52 \pm 0.1$ . This is to be compared with the partial dimensions of the one-dimensional projections of the object on both axes which are obtained as  $D_{\text{box}}^{(x)} = 0.78 \pm 0.06$ ,  $D_{\text{box}}^{(y)} = 0.83 \pm 0.06$ . The results support the rule that the dimension of the cloud is twice the dimension of the projection. The numerical values of the dimensions  $D_{\text{box}}^{(x)}$  and  $D_{\text{box}}^{(y)}$  are, however, slightly smaller than the box dimension of the saddle ( $D_{\text{box}} \approx 0.9$ ). We believe that the reason is a rather slow convergence which can be understood as follows. The partial dimensions of the saddle  $D_0^{(u)}$  and  $D_0^{(s)}$  are the dimensions of the saddle's projections along the stable and unstable manifold, respectively. Since these manifolds are only slightly bent, it is difficult to distinguish these projections from the ones taken along the  $x$  and  $y$  axes. Thus a numerical calculation of  $D_{\text{box}}^{(x)}$  and  $D_{\text{box}}^{(y)}$  with a usual accuracy yields results differing from the exact ones which could only be obtained by an extremely high resolution.

## V. SUMMARY AND CONCLUSIONS

The main points of the method proposed for reconstructing chaotic saddles from experimental time series based on the creation of a long signal with transient properties can be summarized as follows.

- (1) Take an ensemble of time series containing transients to a steady state behavior.
- (2) Locate the attractor of the dynamics in the variable investigated and separate the transient parts.
- (3) Construct truncated time series, i.e., take the points in region II of the signal. Their average length is the reciprocal value of the escape rate from the chaotic saddle. Try different cuttings of the transient pieces so that the results do not depend on details of the truncating procedure.
- (4) Glue the truncated signals together, apply a low-dimensional time-delay coordinate embedding, produce a Poincaré section, and plot the invariant set.
- (5) Apply some simple matching procedure in order to get rid of artificial points (the cloud).
- (6) Apply the usual time-series analysis method to determine quantitative characteristics of the chaotic saddle such as, e.g., dimensions or Lyapunov exponents.

By means of this procedure, chaotic saddles underlying transient chaotic motions can be reconstructed, and their characteristics taken with respect to the natural measure can be determined from time series. We hope that these findings motivate further experimental studies.

It is worth finally briefly mentioning the case of chaotic transients in a Hamiltonian system that appears in the form of *chaotic scattering* [30]. Because of the Hamiltonian character, attractors cannot exist in such systems but chaotic saddles can be and, in fact, are always present if chaotic behavior is observed in scattering. This situation is highly reminiscent of case (3) of dissipative systems (discussed in Sec. II) when the chaotic saddle coexists with an attractor at infinity. Except for the fact that infinity is now not an attractor but rather that part

of the phase space which corresponds to the asymptotic freedom of scattering trajectories, the structure of the chaotic saddle might be quite similar to that of dissipative cases. The main difference is that now an extra symmetry is present which says that stable and unstable directions are essentially equivalent as follows, e.g., from time reversal invariance. Thus we conclude that the method described in this paper can be applied to Hamiltonian cases too, and can be used to reconstruct and characterize transient chaos associated with scattering processes.

## ACKNOWLEDGMENTS

The authors are indebted to H. Kantz for providing them with his work on the calculation of maximal Lyapunov exponents, to J. Vollmer for critical comments on the preliminary version of this paper, and to K. G. Szabó for careful reading of this manuscript. This work has been supported by the Hungarian National Science Foundation (OTKA) under Grant No. 2090, No. T4439, and by the Foundation for Hungarian Higher Education and Research.

- 
- [1] T. Tél, in *Directions in Chaos*, edited by Hao Bai Lin (World Scientific, Singapore, 1990), Vol. 3, p. 149.
  - [2] C. Grebogi, E. Ott, and J. Yorke, *Phys. Rev. Lett.* **48**, 1507 (1982); *Physica (Amsterdam) D* **7**, 181 (1983).
  - [3] H. Kantz and P. Grassberger, *Physica (Amsterdam) D* **17**, 75 (1985).
  - [4] H. E. Nusse and J. Yorke, *Physica (Amsterdam) D* **36**, 137 (1989).
  - [5] C. Grebogi, E. Ott, and J. Yorke, *Phys. Rev. A* **36**, 3522 (1987).
  - [6] P. Cvitanovic, *Phys. Rev. Lett.* **61**, 2729 (1988).
  - [7] T. Tél, *J. Phys. A* **22**, L691 (1989).
  - [8] V. Croquette and C. Poitou, *C. R. Acad. Sci.* **292**, 1353 (1981).
  - [9] F. T. Arecchi, R. Meucci, G. Puccioni, and J. Tredicce, *Phys. Rev. Lett.* **49**, 1217 (1982).
  - [10] P. Bergé and M. Dubois, *Phys. Lett.* **93A**, 365 (1983).
  - [11] F. T. Arecchi and F. Lisi, *Phys. Rev. Lett.* **50**, 1330 (1983).
  - [12] R. W. Rollins and E. R. Hunt, *Phys. Rev. A* **29**, 3327 (1984); R. C. Hilborn, *ibid.* **31**, 378 (1985).
  - [13] R. W. Leven, B. Pompe, C. Wilke, and B. P. Koch, *Physica (Amsterdam) D* **16**, 371 (1985).
  - [14] M. Gorman, P. J. Widmann, and K. A. Robbins, *Phys. Rev. Lett.* **52**, 2241 (1984); *Physica (Amsterdam) D* **19**, 255 (1986); P. J. Widmann, M. Gorman, and K. A. Robbins, *ibid.* **36**, 157.
  - [15] T. L. Carroll, L. M. Pecora, and F. J. Rachford, *Phys. Rev. Lett.* **59**, 2891 (1987); *Phys. Rev. A* **40**, 377 (1989); **40**, 4149 (1989); *J. Appl. Phys.* **64**, 5396 (1988); T. L. Carroll, F. J. Rachford, and L. M. Pecora, *Phys. Rev. B* **38**, 2938 (1988).
  - [16] Z. J. Kowalik, M. Franaszek, and P. Pieranski, *Phys. Rev. A* **37** (1988).
  - [17] F. Papoff, D. Dangoisse, E. Poite-Hanoteau, and P. Glorieux, *Opt. Commun.* **67**, 358 (1988); D. Dangoisse, P. Glorieux, and D. Hennequin, *Phys. Rev. Lett.* **57**, 2657 (1986).
  - [18] W. L. Ditto *et al.*, *Phys. Rev. Lett.* **63**, 923 (1989).
  - [19] R. Stoop and J. Parisi, *Phys. Rev. A* **43**, 1802 (1991).
  - [20] R. W. Leven, M. Selent, and D. Uhlrandt (private communication).
  - [21] T. Vicsek, *Fractal Growth Phenomena* (World Scientific, Singapore, 1989).
  - [22] P. Grassberger and I. Proccacia, *Physica (Amsterdam) D* **9**, 189 (1983).
  - [23] Z. Kovács and T. Tél, *Phys. Rev. Lett.* **64**, 1617 (1990); and (unpublished).
  - [24] K. Pawelzik and H. G. Schuster, *Phys. Rev. A* **35**, 481 (1987).
  - [25] R. W. Leven and D. Uhlrandt, *Chaos Soliton Fractals* **2**, 471 (1992).
  - [26] A. Wolf, J. B. Swift, L. Swinney, and A. Vastano, *Physica D* **16**, 285 (1985).
  - [27] J. P. Eckmann, S. O. Kamphorst, D. Ruelle, and S. Ciliberto, *Phys. Rev. A* **34**, 4971 (1986).
  - [28] U. Parlitz, *Int. J. Bif. Chaos* **2**, 155 (1992).
  - [29] H. Kantz (unpublished).
  - [30] U. Smilansky, in *Chaos and Quantum Physics* (North-Holland, Amsterdam, 1992), p. 121.



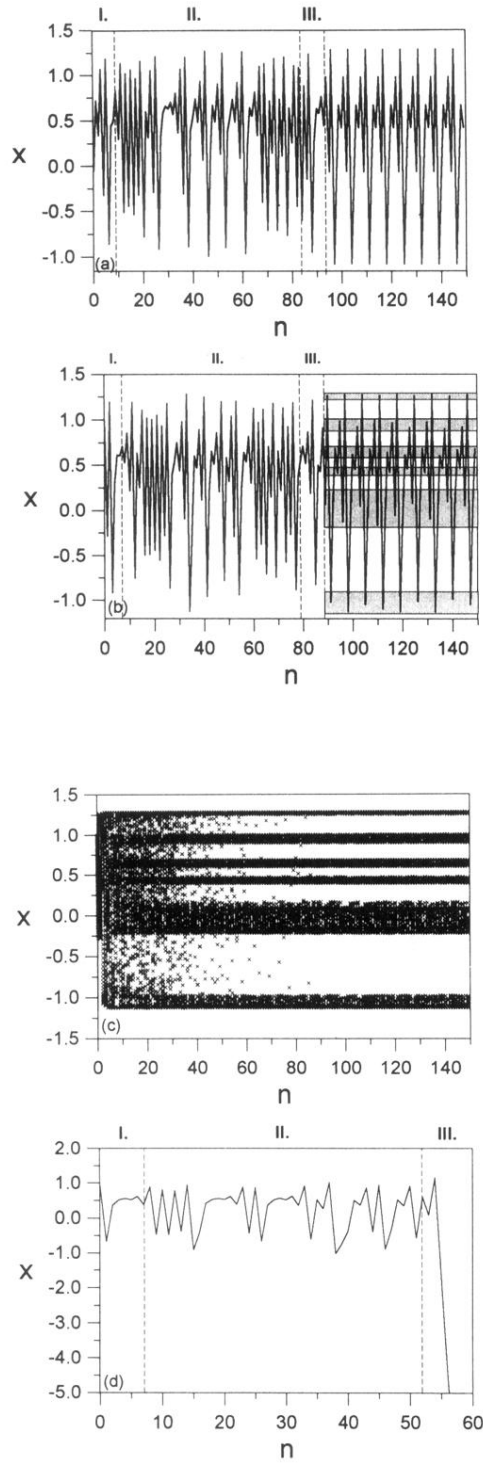


FIG. 1. Typical transient signals generated by variable  $x$  of the Hénon map. (a) Signal settling down on a period-6 attractor,  $a = 1.240$ ,  $b = 0.3$ . The initial point is  $x_0 = 0.92$ ,  $y_0 = 0$ . (b) Signal settling down on a multipiece chaotic attractor,  $a = 1.2715$ ,  $b = 0.3$ . The initial point is  $x_0 = 0.06$ ,  $y_0 = 0$ . The shaded stripes represent the projection of the seven-piece chaotic attractor to the  $x$  axis. (c) An ensemble of 200 transient chaotic trajectories belonging to uniformly distributed initial points in the interval  $|x| < 0.5$ ,  $y = 0$  at the same parameters as in (b). (d) Signal going to infinity at parameters  $a = 2.0$  and  $b = 0.3$ . The starting point is  $x_0 = 0.930\ 092$ ,  $y_0 = 0$ .